Research in Astronomy and Astrophysics, 24:065021 (20pp), 2024 June https://doi.org/10.1088/1674-4527/ad44f0

Analysis of the Impact of the Blazhko Effect Both on the Van Hoof Effect and Radial Velocity Amplitude in the Star RR Lyr

Y. El jariri[1], F.L. Sefyani[2], A. Benhida[2], Z. Benkhaldoun[1], K. Kolenberg[3], K. Chafouai[1], A. Habib[1], and M. Sabil[1,4]
[1] Observatoire de l'Oukaimeden, LPHEA, FSSM, Université Cadi Ayyad, Marrakech, 2390, Morocco; eljaririyoussef2002@gmail.com
[2] Observatoire de l'Oukaimeden, LPHEA, FSTG, Université Cadi Ayyad, Marrakech, 549, Morocco
[3] Département de physique, Université d'Anvers Avenue Groenenborger 171, Anvers, 2020, Belgium
[4] LICPM, ENSA-BM, Université Sultan Moulay Slimane, Beni-Mellal, 23020, Morocco
Received 2023 October 29; revised 2024 March 15; accepted 2024 April 19; published 2024 June 4

Abstract

The Van Hoof effect is a phase shift existing between the radial velocity curves of hydrogen and metallic lines within the atmosphere of pulsating stars. In this article, we present a study of this phenomenon through the spectra of the brightest pulsating star RR Lyr of RR Lyrae stars recorded for 22 yr. We based ourselves, on the one hand, on 1268 spectra (41 nights of observation) recorded between the years 1994 and 1997 at the Observatory of Haute Provence (OHP, France) previously observed by Chadid and Gillet, and on the other hand on 1569 spectra (46 nights of observation) recorded at our Oukaimeden Observatory (Morocco) between 2015 and 2016. Through this study, we have detected information on atmospheric dynamics that had not previously been detected. Indeed, the Van Hoof effect which results in a clear correlation between the radial velocities of hydrogen and those of the metallic lines has been observed and analyzed at different Blazhko phases. A correlation between the radial velocities of different metallic lines located in the lower atmosphere has been observed as well. For the first time, we were able to show that the amplitude of the radial velocity curves deduced from the lines of hydrogen and that of Fe II (λ4923.921 Å) increases toward the minimum of the Blazhko cycle and decreases toward the maximum of the same Blazhko cycle. Furthermore, we found that the Van Hoof effect is also modulated by the Blazhko effect. Thus, toward the minimum of the Blazhko cycle the Van Hoof effect is more visible and at the maximum of the Blazhko cycle, this effect is minimal. We also observed the temporal evolution of the amplitudes of the radial velocities of the lower and upper atmosphere. When observed over a long time, we can interpret it as a function of the Blazhko phases.

Key words: stars: atmospheres – stars: variables: RR Lyrae – shock waves – techniques: spectroscopic – techniques: radial velocities – stars: individual (RR Lyr)

1. Introduction

The Van Hoof effect expresses the propagation time of shock waves, which appear in the atmosphere of pulsating stars with each cycle of pulsation. It was discovered in 1953 in the beta Cephei star beta CMa (Van Hoof & Struve 1953). This phenomenon is still a subject of study since it allows us to obtain important information on the kinematics of the atmospheric layers of pulsating stars, which are relatively less well-known. In the star RR Lyr (which is the prototype and brightest star of the RR Lyrae pulsating class of stars), Mathias et al. (1995), for the first time, detected the Van Hoof effect between the metallic lines and those of the Balmer lines of hydrogen, while no Van Hoof effect was observed between the metallic lines. This absence was interpreted by Fokin (1992) using nonadiabatic and nonlinear pulsation models, which describe it in RR Lyrae stars. Mathias et al. (1995) suggested that the absence of the Van Hoof effect between the metallic lines is because they are all formed in the same region. Thus, all the layers concerned are then subjected to approximately the same physical effects and it was thought that the strong shock waves were only present in the upper atmosphere where the nuclei of the hydrogen lines are formed. Later, Chadid & Gillet (1998) detected for the first time the Van Hoof effect between certain metallic lines (Fe II-Fe I, Fe II-Ti II, etc.) in the atmosphere of RR Lyr. A complete theoretical study has been published by Fokin & Gillet (1997) which suggests that a strong shock wave propagates through the lower photospheric layers contrary to the initial theoretical conclusion of Fokin (1992).

In this article, we will highlight the Van Hoof effect that occurs between the different chemical elements constituting the various atmospheric layers of RR Lyr (Fleming 1899) in correlation with the Blazhko effect. The Blazhko effect is characterized by a cyclic variation in the amplitude of the light curve. It was initially discovered by Sergy Blažko in 1907, in the star RW Draconis, an RR Lyrae type star, by noting irregularities in the times when the star reached its maximum brightness (maxima), contrary to expectations for this type of star.

By closely studying observational data, Blažko discovered a cyclic modulation of the times of maxima for RW Draconis over a period of approximately 41.6 days. This meant that the period between two maxima was not constant but varied periodically. Additionally, Blažko noticed that this modulation also affected the amplitude of the star's light curves. The amplitude of brightness variations for RW Draconis also varied cyclically depending on the modulation period. However, for the star RR Lyr, this effect was first detected by Shapley in (1916) with a period of 40.8 days.

We analyzed the spectra recorded at Observatoire de Haute Provence (OHP) from 1994 to 1997 out of a total of 1268 spectra. Similarly, we used a total of 1569 spectra recorded at the Oukaimeden Observatory (Morocco) during the years 2015 and 2016. Note that the Blazhko effect diminished in 2013 (Le Borgne et al. 2014) and we believe that this phenomenon could have effects on the Van Hoof effect compared with studies published on the same OHP database. In Section 2, we describe the detailed analysis of the observations and the process of spectral reduction. Section 3 will be devoted to the detection of the Van Hoof effect within the atmosphere of the star RR Lyr. Section 4 will be reserved for the study of the evolution of the amplitudes of the radial velocity curves deduced from the Fe II and H_β absorption lines. The evolution of their shifts concerning the minimum and maximum of the Blazhko phases will be discussed in Section 5. The discussion and interpretation of the Van Hoof phenomenon and the evolution of radial velocities will be presented in Section 6. A general conclusion on this study highlighting a global vision of the Van Hoof effect and its implications are provided in Section 7. In this article, the Blazhko phases are denoted by ψ, and the pulsation phases are denoted by ϕ.

The pulsation phase ϕ is obtained from the following formula:

$$\phi = \frac{t_{\rm obs} - t_{\max}}{P} \quad \text{where} \tag{1}$$

1. $t_{\rm obs}$ is the moment of observation of the star (in Heliocentric Julian Date, HJD).
2. $t_{\max}$ is the moment corresponding to the maximum intensity of the light due to the pulsation of the star (in HJD).
3. P is the pulsation period (in days).

The Blazhko phase ψ is obtained from the following formula:

$$\psi = \frac{t_{\rm obs} - t_{\rm maxB}}{P_B} \quad \text{where:} \tag{2}$$

1. $t_{\rm obs}$ is the moment of observation of the star (in HJD).
2. $t_{\rm maxB}$ is the moment corresponding to the maximum intensity of the light due to the Blazhko effect (in HJD), obtained from the ephemerides.
3. $P_{\rm B}$ is the period of the Blazhko effect (in days).

2. Observations and Data Analysis

2.1. Observations at the Haute Provence Observatory (OHP) (Observed by Chadid and Gillet)

The ELODIE spectrograph (Baranne et al. 1996) was utilized to acquire the spectra, functioning as a cross-dispersion spectrograph. It was illuminated by a pair of optical fibers connected to the Cassegrain focus of the 1.93 m telescope. The Milton-Roy grating produced a spectrum ranging from 3890 to 6800 Å across 67 orders, with a resolution power of approximately 42,000. The detector employed was a thinned TK1024 CCD with a 24 μm pixel. Exposure times between 300 and 600 s resulted in a signal-to-noise ratio (SNR) exceeding 40. Data reduction, including offset correction (with a precision of approximately 1 e^-), division by the tungsten lamp spectrum, and wavelength calibration using a thorium-argon lamp, occurred promptly after image recording. The automatic procedure generated a calibrated spectrum in the heliocentric rest frame for each order. Additionally, each spectrum was normalized to its continuum with an accuracy of approximately 1% using a polynomial formula. A Gaussian convolution with a Full Width at Half Maximum (FWHM) of 3.5 px was applied to each spectrum. Wavelength scales were adjusted to the stellar frame of RR Lyr, assuming a star velocity $V_* = -73.5\ \mathrm{km\,s^{-1}}$ relative to the barycenter of the solar system. These operations were conducted using the Munich Image Data Analysis System (MIDAS). For a more in-depth understanding, refer to the work of Chadid & Gillet (1996).

2.2. Observations at the Oukaimeden Observatory

The spectral data were acquired using the Echelle spectrograph, equipped with eShel fiber optics developed by Shelyak Instruments (Thizy & Cochard 2010). The eShel system comprises an F/6 fiber injection and guiding unit, a 50 μm fiber optic, a ThAr calibration unit, and a ladder spectrograph (125 mm F/5 collimator, R2 ladder grating, cross-dispersion, 85 mm F/1.8 lens). The spectrograph was mounted on a C14 Celestron telescope at the Oukaimeden Observatory situated at an altitude of 2700 m in the High Atlas Mountains, 78 km south of Marrakech. The pixel size is 6.8 μm, and the spectral dispersion is 16 Å mm^{-1} or 0.1 Å px^{-1}. Spectra were obtained across a broad section of the visible range (from 4100 to 7200 Å), spanning orders 32 to

52, and exhibiting a resolving power of approximately 12,000. With an exposure time of 300 s, the SNR exceeds 30. The adopted temporal resolution is $\Delta t/P = 0.6\%$. The data underwent reduction using the free and open-source astronomy software AudeLA. Wavelengths are reported in the rest frame of RR Lyr, considering a star velocity V_* relative to the barycenter of the solar system at -73.5 km s^{-1} (Chadid & Gillet 1996). Spectra were subjected to filtering using a Gaussian filter with a standard deviation of 0.6 pixels. For additional information, please consult the article by Gillet et al. (2016).

2.3. Graphical Representation of Data

The graphical representation of the data was carried out using the TK-SPECTRO graphical interface within the PHEA Laboratory located at the Semlalia Faculty of Sciences of Cadi Ayyad University in Marrakech (El jariri et al. 2023). Thanks to this graphical interface, the Doppler shift of the wavelengths was corrected by considering the velocity $V_* = -73.5$ km s^{-1} of the RR Lyr star relative to the barycenter of the solar system (Chadid & Gillet 1996), thus allowing the calculation of both pulsation phases and Blazhko phases. These calculations were performed using the ephemerides from Table 2 of the article by Gillet et al. (2019), detailed below in HJD.

We used the following Blazhko ephemeris corresponding at 2015 November 27 at 19 hr 43 UT (Gillet et al. 2017):

HJD(max. light ampl.) = 2457354.322+39.0E

From Dalmazio's (1992) investigations based on 1082 observed RR Lyrae magnitudes in 1991, Chadid & Gillet (1996) determined the ephemeris of the Blazhko phase:

HJD(max. light ampl.) = 2448549.296+39.03E

This ephemeris has been used for all spectra recorded before 1995. For the observations carried out between 1995 August and 1997 August, Chadid & Gillet (1996) had to use the observations of 950 mag of RR Lyr by Dalmazio (1995) obtained in 1994 to derive ephemeris:

HJD(max. light ampl.) = 2449631.312+39.03E

Based on the analysis of Le Borgne et al. (2014), the period of Blazhko cycle is 39.03 days for HJD between 2448012 and 2450000 and 39.06 days for HJD between 2450224 and 2452926.

The pulsation phases between 1994 and 1997 were calculated using the ephemerides provided by Chadid & Gillet (1997):

HJD (max. light) = 2446654.368+0.566839E

Furthermore, for the years 2015 and 2016, when calculating the pulsation phases for each considered night, we chose the date of maximum luminosity of that night's pulsation cycle, even if it occurred at the beginning of the night or just after its end, as indicated below:

HJD (max. light) = 2457324.335+0.5667975E (2015)

HJD (max. light) = 2457559.538+0.566793E (2016)

The radial velocities are deduced by this interface based on the Gaussian adjustment of absorption lines from various chemical elements. Tk-Spectro automatically isolates absorption lines below the continuum and injects them into a Gaussian function for adjustment. This process involves multiple iterations to choose the best Gaussian fit and calculate its center of mass, thereby deducing the radial velocity through the Doppler effect. Additionally, Tk-Spectro provides the option to display the Gaussian adjustment on the graph, allowing the user to verify if the selected lines correspond well to the adjustment. In case of discrepancies, the user can adjust the wavelength interval through Tk-Spectro's graphical interface to minimize differences between the lines and their Gaussian fit. Another advantage of Tk-Spectro is the detection of line splitting, followed by the injection of each component into a Gaussian function to calculate the radial velocity of the stronger component (details on the radial velocity calculations are provided in Section 2.2.6 of the article by El jariri et al. 2023). Thus, from these data, we were able to determine the amplitudes of radial velocity curves as well as the maximal radial velocity differences between the H_β and Fe II (λ4923.921 Å), lines. The calculations of maximum and minimum radial velocities, amplitudes, and differences between the maxima of Fe II and H_β are summarized in Table 1 below. We have also plotted the RV-RV diagrams of the radial velocities of Fe II (λ4923.921 Å) as a function of the radial velocities of the following elements: Fe II (λ4549.214 Å), Fe I (λ4920.509 Å), Ba II (λ4934.076 Å), Ti II (λ5188.7 Å) and H_β (λ4861.3 Å). We have represented the radial velocities as a function of the pulsation phases and the Blazhko phases, the amplitudes of the velocity curves and the shifts between them for Fe II (λ4923.921 Å) and H_β (λ4861.3 Å) as a function of Blazhko phases and observation dates. In the present work, we took the value of the velocity of the stellar resting mark of the star RR Lyr with respect to the barycenter of the solar system: $V_* = -73.5$ km s^{-1}(Chadid & Gillet 1996). The series of observation nights, the errors of radial velocities $(\Delta \mathrm{RV})_{\mathrm{Error}}$, the SNRs, the pulsation ranges and the Blazhko phases are listed in Table 2. The amplitudes of the radial velocity curves of Fe II (λ4923.921 Å) and H_β (λ4861.3 Å) and their shifts as a function of the Blazhko phases are detailed in Section 5.

3. Van Hoof Effect between Metallic Lines and Hydrogen

In this section, we will represent the velocity-velocity diagrams in the order of the Blazhko phases for Fe II (λ4549.214 Å) (Figure 1), Fe I (λ4920.509 Å) (Figure 2), Ba II (λ4934.076 Å) (Figure 3), Ti II (λ5188.7 Å) (Figure 4) and H_β (λ4861.3 Å) (Figure 5) compared to Fe II (λ4923.921 Å). The series of observation nights represented by these graphs are: two series of two consecutive nights: 1995 September 5 and 6 and 1996 August 9 and 11, seven series of the following three

Table 1

Maximum ($RV_{\rm max}$) and Minimum ($RV_{\rm min}$) Radial Velocities, Amplitudes of Radial Velocity Curves, and Differences between the Peaks of Maximum Radial Velocities, Deduced from Fe II and H_β Lines Corresponding to Different Blazhko Phases

Night Series	HJD (+2400000)	ψ	$RV_{\rm max}$ ($0.80 \leqslant \phi \leqslant 0.95$)		$RV_{\rm min}$ ($0.96 \leqslant \phi \leqslant 1.15$)		RV Amplitude		$\Delta RV_{\rm max}$ Peaks
			Fe II	H_β	Fe II	H_β	Fe II	H_β	
1994 Aug 3-4-5	49568.381-49570.606	0.41	30.38 ± 1.22	44.28 ± 1.03	−29.01 ± 1.22	−42.04 ± 1.03	59.39 ± 2.44	86.32 ± 2.06	13.9 ± 2.25
1995 Sep 5-6	49966.32-49967.515	0.6	30.10 ± 1.07	47.67 ± 1.03	−34.12 ± 1.07	−49.05 ± 1.03	64.22 ± 2.14	96.72 ± 2.06	17.57 ± 2.1
1996 Jun 24-25-26	50259.376-50261.505	0.11	23.51 ± 1.08	38.56 ± 0.98	−28.37 ± 1.08	−50.5 ± 0.98	51.88 ± 2.16	89.06 ± 1.96	15.05 ± 2.06
1996 Jul-Aug 31-1-2	50296.334-50298.623	0.05	26.01 ± 1.18	40.47 ± 1.03	−30.74 ± 1.18	−47.65 ± 1.03	56.75 ± 2.36	88.12 ± 2.06	14.46 ± 2.21
1996 Aug 9-11	50305.343-50307.638	0.29	28.21 ± 1.06	42.66 ± 0.96	−27.03 ± 1.06	−43.89 ± 0.96	55.24 ± 2.12	86.55 ± 1.92	14.45 ± 2.02
1997 Aug 5-6-7	50666.392-50668.633	0.53	30.10 ± 1.21	47.57 ± 1.01	−32.69 ± 1.21	−49.57 ± 1.01	62.79 ± 2.42	97.14 ± 2.02	17.47 ± 2.22
1997 Aug 8-9-10	50669.325-50671.543	0.6	30.36 ± 1.17	46.81 ± 0.99	−32.89 ± 1.17	−48.08 ± 0.99	63.25 ± 2.34	94.89 ± 1.98	16.45 ± 2.16
1997 Aug-Sep 29-30-31	50690.525-50692.636	0.14	25.17 ± 1.12	38.35 ± 0.96	−24.94 ± 1.12	−44.41 ± 0.96	50.11 ± 2.24	82.76 ± 1.92	13.18 ± 2.08
2015 Oct 28-29-30	57324.357-57326.48	0.26	35.12 ± 2.07	47.88 ± 1.89	−31.56 ± 2.07	−41.33 ± 1.89	66.68 ± 4.14	89.21 ± 3.78	12.76 ± 3.96
2016 Jun 19-20-21-22	57559.532-57562.57	0.3	32.32 ± 2.18	48.82 ± 1.82	−30.11 ± 2.18	−49.73 ± 1.82	62.43 ± 4.36	98.55 ± 3.64	16.5 ± 4

Table 2
Series of Measurement Nights, with their Dates, Pulsation Phase Intervals, Blazhko Phases, Number of Spectra for Each Night, $(\Delta RV)_{Error}$ in km s^{-1} and SNR

Night series	Date (yyyy mm dd)	ϕ Interval	ψ	Number of Spectra	$(\Delta RV)_{Error}$						SNR					
					Fe II	Fe II	Fe I	Ba II	Ti II	H_β	Fe II	Fe II	Fe I	Ba II	Ti II	H_β
	1994 Aug 3-4	0.779-1.11	0.39	26												
1	1994 Aug 4-5	0.466-0.932	0.41	35	1.22	1.14	1.13	1.18	1.01	1.03	42	39	40	42	41	41
	1994 Aug 5-6	1.185-1.704	0.44	34												
2	1995 Sep 5-6	0.806-1.375	0.59	48	1.07	1.3	1.11	1.21	1.02	1.03	38	37	38	38	37	37
	1995 Sep 6-7	0.681-0.915	0.61	12												
	1996 Jun 24-25	0.823-1.22	0.08	30												
3	1996 Jun 25-26	0.547-0.978	0.11	34	1.08	1.16	1.19	1.13	1.01	0.98	40	41	40	40	39	38
	1996 Jun 26-27	0.306-0.579	0.13	30												
	1996 Jul-Aug 31-1	1.025-1.536	0.03	52												
4	1996 Aug 1-2	0.787-1.307	0.05	56	1.18	1.13	1.15	1.15	1.04	1.03	40	37	40	40	40	41
	1996 Aug 2-3	0.812-1.065	0.08	20												
5	1996 Aug 9-10	0.919-1.428	0.26	54	1.06	1.16	1.16	1.11	0.97	0.96	39	36	39	39	38	37
	1996 Aug 11-12	0.431-0.969	0.31	36												
	1997 Aug 5-6	0.896-1.326	0.5	31												
6	1997 Aug 6-7	0.546-1.091	0.53	58	1.21	1.21	1.13	1.19	1.01	1.01	39	39	39	39	40	38
	1997 Aug 7-8	1.304-1.85	0.55	56												
	1997 Aug 8-9	1.071-1.611	0.58	60												
7	1997 Aug 9-10	0.832-1.377	0.6	47	1.17	1.12	1.17	1.13	1	0.99	39	37	39	40	39	38
	1997 Aug 10-11	0.603-0.983	0.63	36												
	1997 Aug 29-30	1.093-1.614	0.11	51												
8	1997 Aug 30-31	0.858-1.45	0.14	65	1.12	1.06	1.13	1.15	0.99	0.96	41	38	41	41	40	40
	1997 Aug-Sep 31-1	0.685-1.197	0.17	60												
	2015 Oct 28-29	1.037-1.302	0.24	42												
9	2015 Oct 29	0.666-1.052	0.26	57	2.07	2.07	2.21	2.17	1.9	1.89	32	33	31	21	33	32
	2015 Oct 30	0.412-0.784	0.28	60												
	2016 Jun 19-20	0.726-1.135	0.26	66												
10	2016 Jun 20-21	0.516-0.989	0.29	75	2.18	⋯	2.26	2.51	⋯	1.82	30	⋯	23	29	⋯	34
	2016 Jun 21	1.27-1.427	0.31	23												
	2016 Jun 22-23	1.136-1.35	0.34	35												

Note. Three periods (⋯) signify that the corresponding lines are either unusable due to excessive noise or that they do not exist.

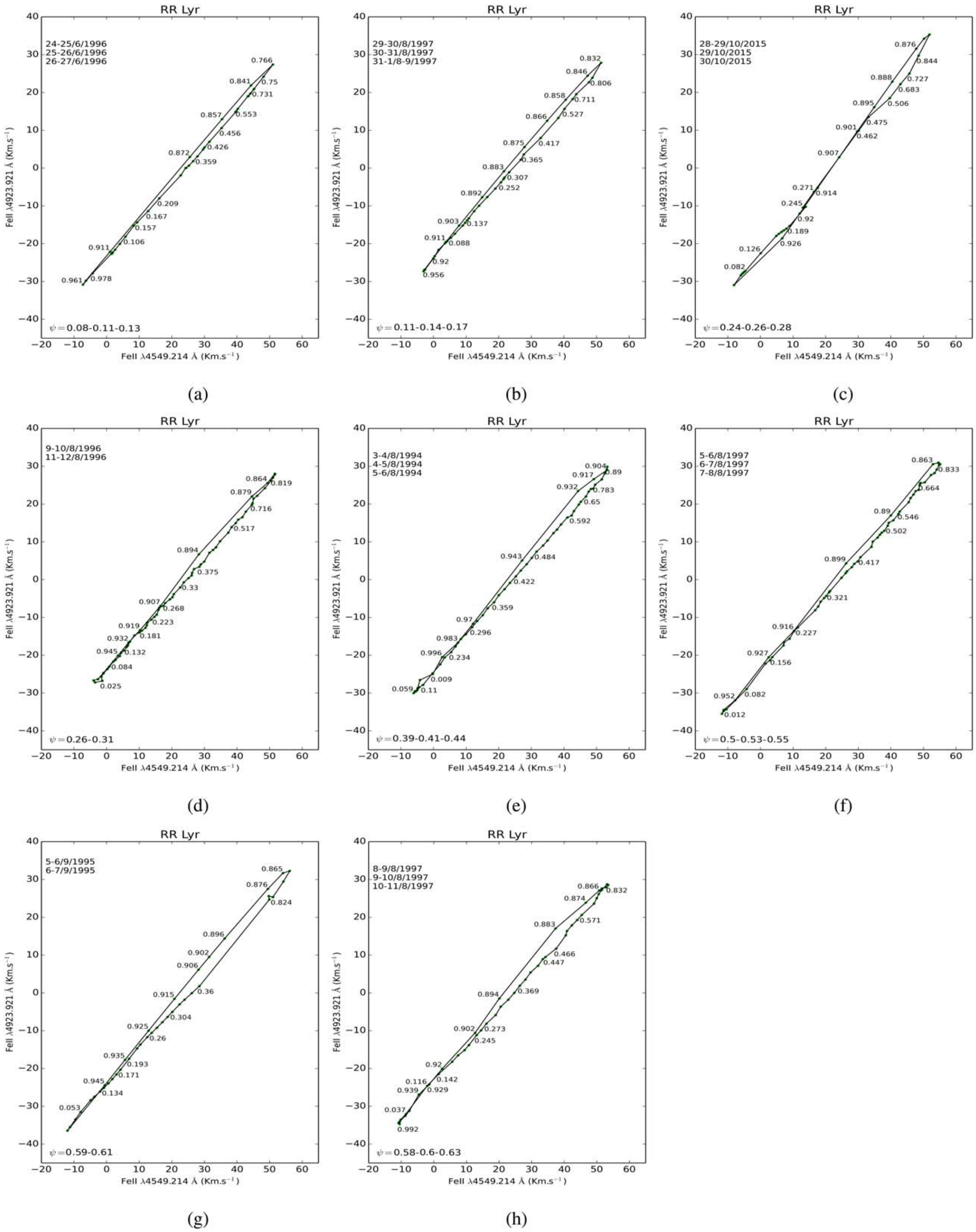

Figure 1. (a), (b), (c), (d), (e), (f), (g), and (h): Radial velocities of Fe II (λ4923.921 Å) plotted against those of Fe II (λ4549.214 Å). Certain pulsation phases are also indicated on the curves. At the top left are the dates of the nights of each series (dd/mm/yyyy), and at the bottom left the Blazhko phases corresponding to each night.

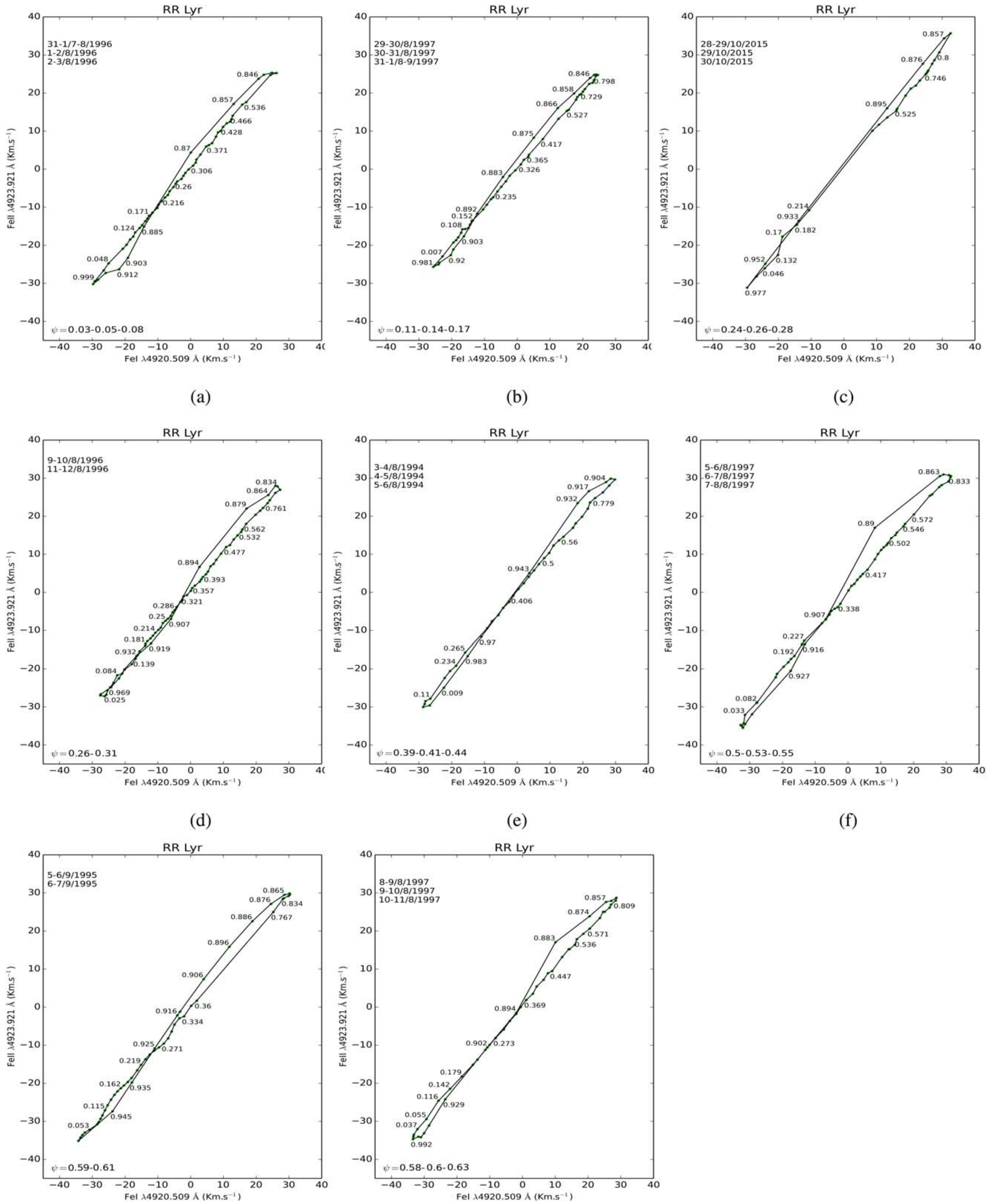

Figure 2. (a), (b), (c), (d), (e), (f), (g), and (h): Same as Figure 1, but for Fe II (λ4923.921 Å) and Fe I (λ4920.509 Å).

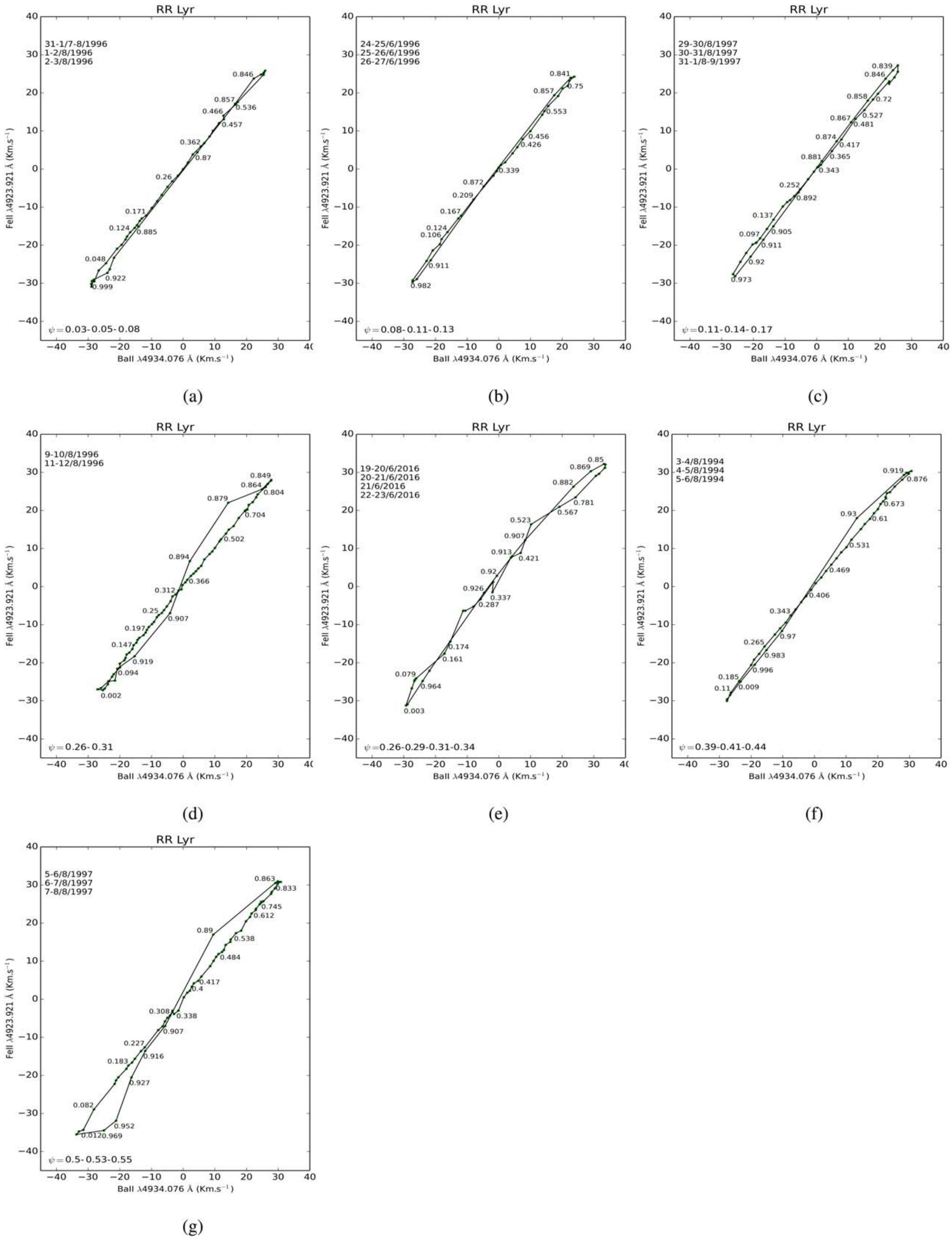

Figure 3. (a), (b), (c), (d), (e), (f), and (g): Same as Figure 1, but for Fe II (λ4923.921 Å) and Ba II (λ4934.076 Å).

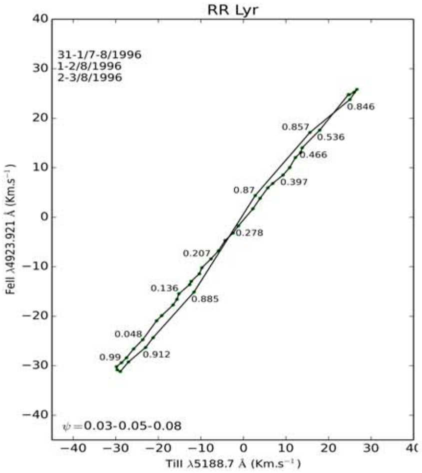

(a)

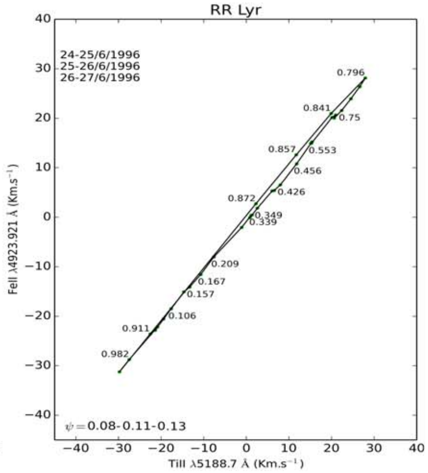

(b)

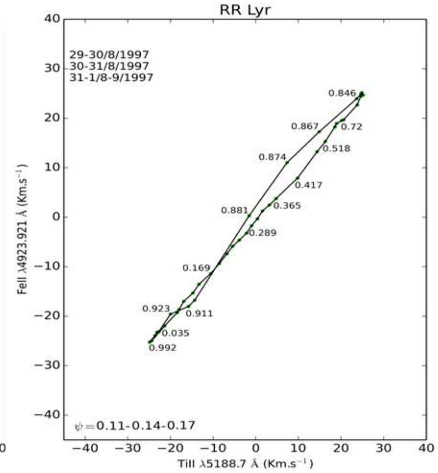

(c)

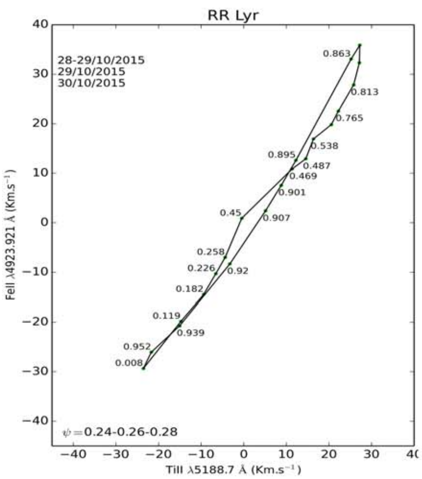

(d)

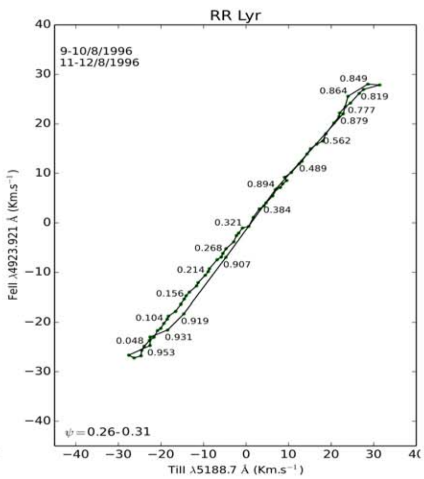

(e)

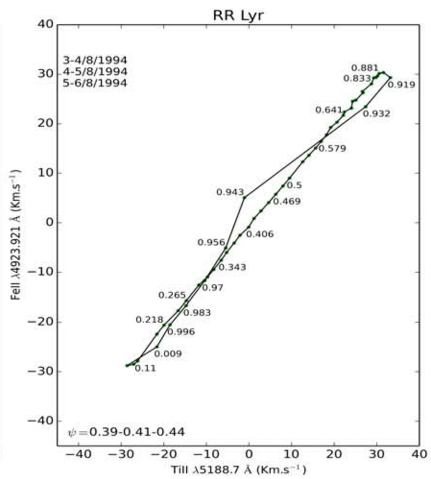

(f)

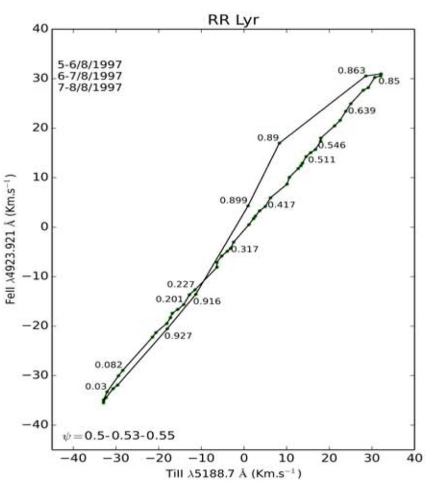

(g)

Figure 4. (a), (b), (c), (d), (e), (f), and (g): Same as Figure 1, but for Fe II (λ4923.921 Å) and Ti II (λ5188.7 Å).

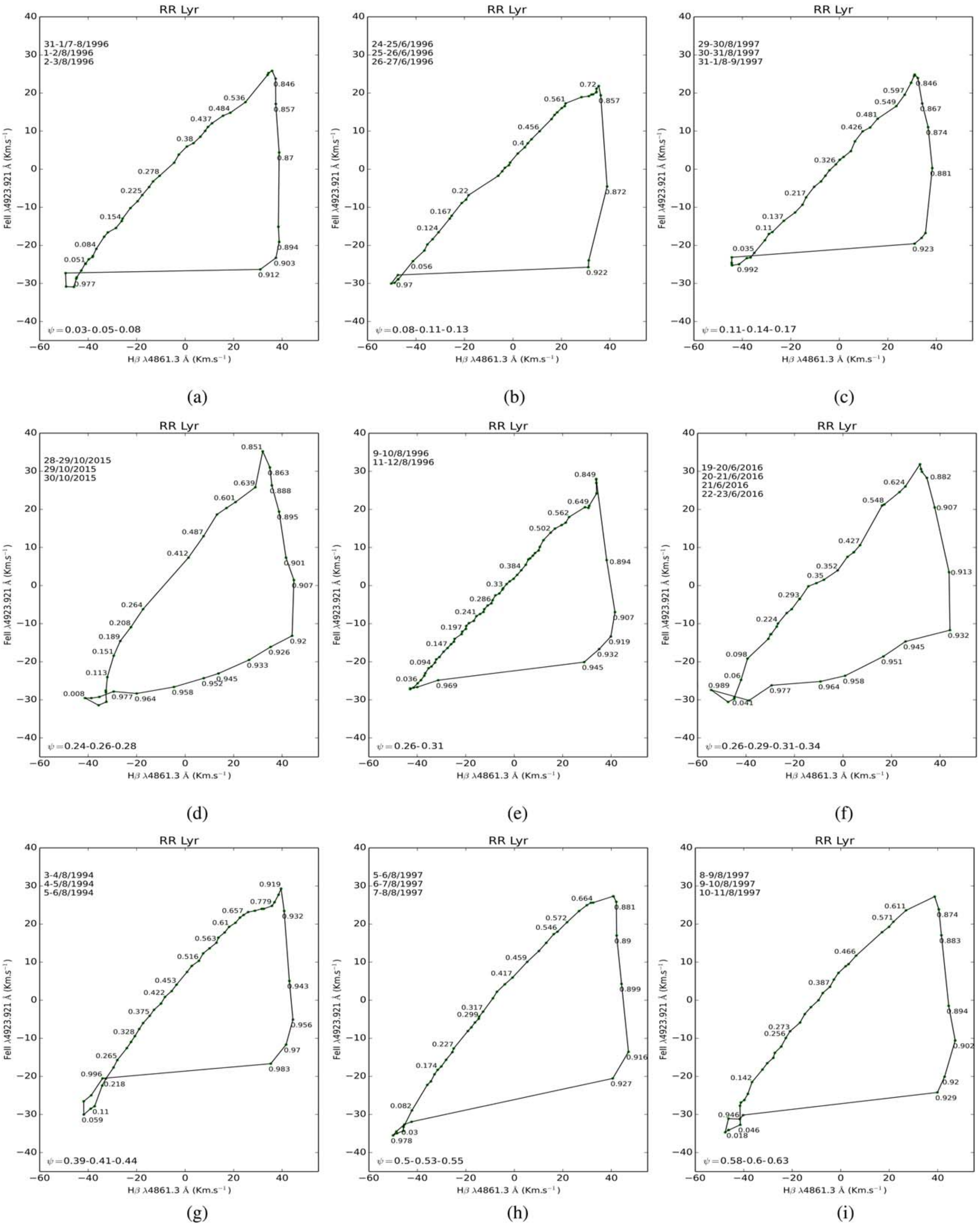

Figure 5. (a), (b), (c), (d), (e), (f), (g), (h), and (i): Same as Figure 1, but for FeII(λ4923.921 Å) and H_β (λ4861.3 Å).

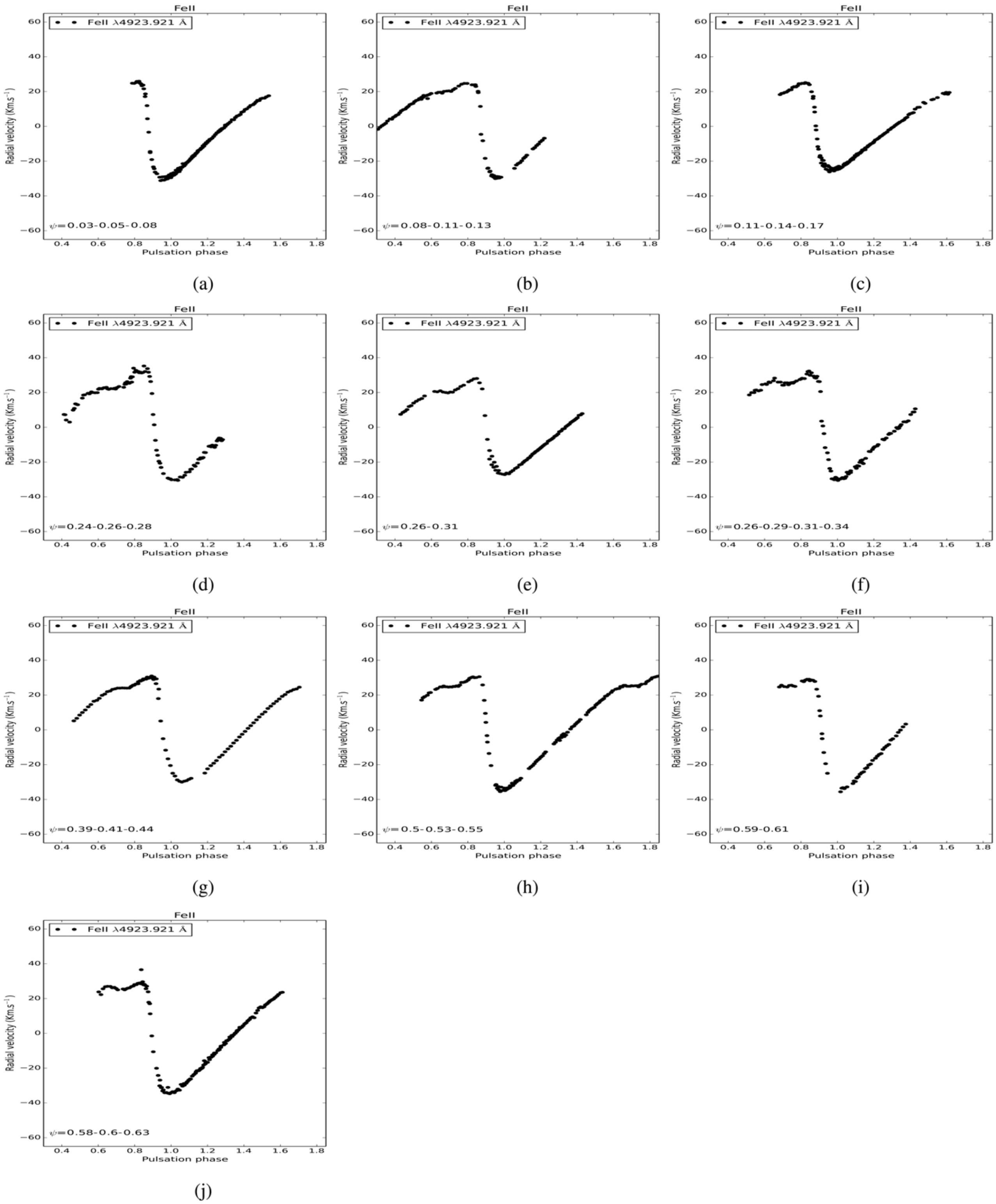

Figure 6. Radial velocity curves deduced from the Fe II line (λ4923.921 Å), corresponding to 10 different Blazhko phases, ordered in ascending order and indicated at the bottom left of each plot, plotted as a function of pulsation phases. Each radial velocity curve is constructed from the series of nights which describe a complete period of pulsation. (Dates of the series of nights are indicated in Table 2).

consecutive nights: 1994 August 3, 4, and 5, 1996 July 31, August 1 and 2, 1996 June 24, 25, and 26, 1997 August 5, 6, and 7, 1997 June 8, 9, and 10, 1997 August 29, 30, and 31, and 2015 October 28, 29, and 30, and a series of four consecutive nights: 2016 June 19, 20, 21, and 22. The pulsation phases of these series make it possible to describe a complete pulsation cycle of RR Lyr which has a period P of 13 hr 36 minutes. The pulsation phase ranges of the night series and the corresponding Blazhko phases are noted in Table 2. The Blazhko phases correspond to maximum, minimum and intermediate phases.

3.1. Fe II (λ4923.921 Å)—Fe II (λ4549.214 Å) diagram

We observe that the radial velocity shift is absent on graphs (a), (b), (d) and (f) of Figure 1 ($(\Delta RV)_{Error} \approx 1.14$ km s^{-1}) corresponding to the Blazhko phases $\psi \approx 0.11$, $\psi \approx 0.14$, $\psi \approx 0.29$, and $\psi \approx 0.53$ respectively. For the graphs in (c), (e), (g), and (h) of Figure 1 corresponding to the Blazhko phases $\psi \approx 0.26$, $\psi \approx 0.41$, $\psi \approx 0.60$, and $\psi \approx 0.60$ respectively, we highlight the existence of a slight shift between the curves of the radial velocities. This confirms the presence of the metallic Van Hoof effect between Fe II (λ4923.921 Å) and Fe II (λ4549.214 Å) around the pulsation phase $\phi \approx 0.88$. For this graph it is quite clear that the diagram is counterclockwise, which means that the variation of the velocity curve of Fe II (λ4923.921 Å) is late compared to that of Fe II (λ4549.214 Å).

Furthermore, the analysis of the radial velocities of Fe II (λ4549.214 Å) reveals high values (an average value is about 20 km s^{-1}), resulting from shock waves in the stellar atmosphere that increase the temperature and partially ionize Fe I into Fe II. The absorption lines of Fe I decrease in favor of those of Fe II. During the pulsation phase from $\phi = 0.90$ to $\phi = 0.95$, the Fe II line (λ4923.921 Å) exhibits a splitting at phase $\phi = 0.941$ (Sefyani et al. 2017), marking the minimum stellar compression radius (Chadid & Gillet 1996) and a null radial velocity of its photosphere, with a reversal of radial velocity during expansion.

Another Fe II (λ4549.214 Å) line shows a splitting at phase $\phi = 0.903$, with a time difference of approximately 30 minutes (Sefyani et al. 2018), marking the attainment of the maximum radial compression velocity of the star (Chadid & Gillet 1996). This line corresponds to ions moving between −10 and 55 km s^{-1}, indicating an outward motion. The Fe II (λ4923.921 Å) line corresponds to ions between −35 and 35 km s^{-1}, with splitting at phase $\phi = 0.941$, indicating an almost null radial velocity, showing both outward and inward motion. The difference in the splitting phase of these two lines is crucial for interpreting velocity variations. These two lines originate from different layers, and the study of the thermodynamic conditions of the atmosphere will contribute to understanding this phenomenon.

3.2. Fe II (λ4923.921 Å)—Fe I (λ4920.509 Å) diagram

For the graphs (e), (f) and (h) of Figure 2 corresponding to the Blazhko phases $\psi \approx 0.41$, $\psi \approx 0.53$ and $\psi \approx 0.60$ respectively, we highlight the existence of a shift between the radial velocity curves which confirms the presence of the metallic Van Hoof effect between Fe II (λ4923.921 Å) and Fe I (λ4920.509 Å) around the pulsation phases $\phi \approx 0.93$, $\phi \approx 0.89$, and $\phi \approx 0.88$ respectively. We observe that the shift is slight on graphs (a), (b), (c), (d), and (g) corresponding to the Blazhko phases $\psi \approx 0.05$, $\psi \approx 0.14$, $\psi \approx 0.26$, $\psi \approx 0.29$, and $\psi \approx 0.60$ respectively. Thus graph (e) is a confirmation of the graph in Figure 2 from the article Chadid & Gillet (1998). The variation of the velocity curves of Fe II lags behind that of Fe I because the pattern is counterclockwise.

3.3. Fe II (λ4923.921 Å)—Ba II (λ4934.076 Å) diagram

Figure 3 represents the graphs of the radial velocity curves of Fe II as a function of Ba II. We observe that the Van Hoof effect is quite evident in graphs (d) and (g) around the pulsation phases $\phi \approx 0.879$ and $\phi \approx 0.89$, corresponding to the Blazhko phases $\psi \approx 0.29$ and $\psi \approx 0.53$ (minimum Blazhko), respectively. A slight shift is observed on the graph (e) around $\phi \approx 0.88$ and corresponds to $\psi \approx 0.29$ and (f) (same graph obtained by Chadid & Gillet (1998) (Figure 3)), around $\phi \approx 0.93$ and corresponding to $\psi \approx 0.41$ (close to minimum Blazhko). But for the maximum Blazhko $\psi \approx 0.05$, $\psi \approx 0.11$, and $\psi \approx 0.14$, we notice the absence of the Van Hoof effect on graphs (a), (b), and (c) respectively. The patterns are depicted in a counterclockwise direction, which means that the variation in the velocity curves of Fe II lags behind those of Ba II.

3.4. Fe II (λ4923.921 Å)—Ti II (λ5188.7 Å) diagram

For the graphs in Figure 4, we observe the absence of the Van Hoof effect in graphs (a), (b), and (e), corresponding to phases $\psi \approx 0.05$ (maximum Blazhko phase), $\psi \approx 0.11$, and $\psi \approx 0.29$, respectively. However, in graphs (c), (d), and (f), which correspond to phases $\psi \approx 0.14$, $\psi \approx 0.26$, and $\psi \approx 0.41$, respectively, we notice a slight shift in the velocity curves around $\phi \approx 0.87$. The Van Hoof effect is relatively clear in graph (g) associated with $\psi \approx 0.53$, around $\phi \approx 0.89$. The direction of the diagram is counterclockwise, confirming that the variation of the velocity curves of Fe II lags those of Ti II.

3.5. Fe II (λ4923.921 Å)—H_β (λ4861.3 Å) diagram

The Van Hoof effect is well marked on graphs (a), (b), (c), (d), (e), (f), (g), (h), and (i) of Figure 5 corresponding to the Blazhko phases $\psi \approx 0.05$, $\psi \approx 0.11$, $\psi \approx 0.14$, $\psi \approx 0.26$, $\psi \approx 0.29$, $\psi \approx 0.29$, $\psi \approx 0.41$, $\psi \approx 0.53$, and $\psi \approx 0.60$ by the existence of a large width along the $y = -x$-axis around $\phi \approx 0.91$, that is to say during the strong acceleration of the atmospheric layers outwards. The schematic curve is clockwise, which means that the variation of the velocity curves of H_β lags behind those of the Fe II lines. This has already been observed in the case of β Cephei star α Lupi (Mathias & Gillet 1993) and was only the consequence of the different altitudes of the regions of formation of the lines.

Important Note:

The most striking feature, observed in Figures 1–5, is that the amplitude of the radial velocity curves is greater when the Blazhko phases are minimal ($\psi \approx 0.5$) and smaller when the Blazhko phases are maximal ($\psi \approx 0.0$) along the $y = x$-axis.

4. The Radial Velocity Curve

Figures 6 and 7 show the radial velocity curves of RR Lyr obtained from the Gaussian fitting of the Fe II (λ4923.921 Å) and the H_β (λ4861.3 Å) lines, respectively. These calculations were carried out during 10 Blazhko phases: $\psi \approx 0.41$, $\psi \approx 0.6$, $\psi \approx 0.11$, $\psi \approx 0.05$, $\psi \approx 0.29$, $\psi \approx 0.53$, $\psi \approx 0.6$, $\psi \approx 0.14$, $\psi \approx 0.26$ and $\psi \approx 0.29$ corresponding to the series of nights listed in Table 2 in chronological order respectively. Each series defines a complete pulsation period (The errors $(\Delta\mathrm{RV})_{\mathrm{Error}}$ km s^{-1} on the radial velocities are noted on the same Table 2). A phase lag is present between the different Blazhko phases. We also notice that the radial velocity curves of Fe II and H_β show that there is an inverse correlation with the Blazhko phase. The radial velocities decrease around the pulsation phases $0.80 \leqslant \phi \leqslant 0.95$ and also exhibit a decrease in absolute value within the range of $0.96 \leqslant \phi \leqslant 1.15$, when the Blazhko phases are maximum and vice versa, as indicated in Table 1. These findings contradict the conclusions published by Chadid (2000). This is likely due to inaccuracies in the calculations of the Blazhko phases used in her article (Chadid 2000). Our calculations (Table A1 in the Appendix) are in agreement with the calculations made by Gillet et al. (2017, 2019) (Detailed in Table 3).

5. Evolution of the Amplitudes of the Radial Velocity Curves

We will present the evolution of the amplitudes (shift between the maximum and minimum of the radial velocity curves) of the metallic lines and those of H_β as a function of the Blazhko phases and of time. The shift between the maxima of the radial velocity curves between the metallic lines and that of H_β as a function of the Blazhko phases will also be presented.

Figures 8 and 9 below highlight the evolution of the amplitude of the velocity curves of H_β and those of Fe II as a function of the Blazhko phases. We find that the amplitudes of the radial velocity curves of H_β and Fe II (λ4923.921 Å) are inversely correlated with the variations in luminosity amplitudes caused by the Blazhko effect (Figures 8 and 9), where the highest luminosity amplitude is observed during a Blazhko cycle at phase $\psi = 0.0$ (Gillet et al. 2019). Indeed, the amplitudes of the radial velocity curves, for the minimum Blazhko phases (around $\psi \approx 0.5$), are approximately (96.25 ± 2.02) km s^{-1} for H_β and approximately (63.42 ± 2.3) km s^{-1} for Fe II. The amplitudes of the radial velocity curves of H_β and Fe II, for the Blazhko maxima (around $\psi \approx 0.0$), are about (86.65 ± 1.98) km s^{-1} for H_β and about (52.91 ± 2.25) km s^{-1} for Fe II. In comparison, Chadid & Gillet (1996) found a pulsation velocity amplitude, $\Delta\dot{R} = 79.5$ km s^{-1}, or about 58.46 km s^{-1} of the radial velocity amplitude ΔRV for Fe II ($\Delta\dot{R} = p\ \Delta\mathrm{RV}$ with p being the geometrical projection and limb-darkening correction factor (Burki et al. 1982)). Note that Chadid obtained these results on the nights of 1994 August 3, 4 and 5, corresponding to the phase $\psi \approx 0.41$. Preston (2011) measured the magnitude of the radial velocity curve obtained from Fe II absorption lines (λ4923.921 Å) of the stable non-Blazhko star RV Oct and found $\Delta\mathrm{RV} \approx 63$ km s^{-1}. For H_β, Preston found $\Delta\mathrm{RV} \approx 115$ km s^{-1} (value deduced from Figure 2).

All the aforementioned results from our study of RR Lyr, the brightest among RR Lyrae-type stars, reveal that the amplitude variations of radial velocities in relation to the Blazhko phases contradict the findings of Chadid & Preston in 2013 for other stars of the same type, as illustrated in Figure 6 of their paper. This discrepancy could be interpreted by the presence of a higher radiative pressure within the atmospheric layers of RR Lyr, leading to a slowdown in its radial velocity during Blazhko maxima. We have elaborated on this explanation in Section 6 of our article, which differs from what has been observed in stars studied by Chadid & Preston. However, the study conducted by Chadid in 2000 on star the RR Lyr clearly illustrates the amplitude variations of radial velocities derived from Fe II λ4923.921 Å lines based on Blazhko phases (see Figures 1, 2, 3, 4, and 5). The problem with Chadid's study lies in the inaccurate calculations of the Blazhko phases, which skewed the identification of the inverse correlation between the Blazhko phases and the radial velocity amplitudes revealed in our study. Table 3 below presents Chadid's calculated Blazhko phases alongside our own calculated Blazhko phases, which align with the Blazhko phases found by Gillet et al. in (2017) and (2019).

A recent article published by Chadid in 2023 confirms the results of our study. Indeed, Figures 15 and 19 in that article depict RV-RV diagrams of Fe II (λ4923.921 Å) in relation to H_β and Fe II (λ4923.921 Å) in relation to Fe I (λ4920.509 Å) at various Blazhko phases, revealing that the amplitude of these velocity curves is significant during minimal Blazhko phases ($\psi \approx 0.5$), reaching approximately 65.1 km s^{-1} for Fe II and 98 km s^{-1} for H_β. Conversely, the amplitude is low during maximal Blazhko phases ($\psi \approx 0.0$), with around 58 km s^{-1} for Fe II and 81 km s^{-1} for H_β along the $y = x$-axis. This

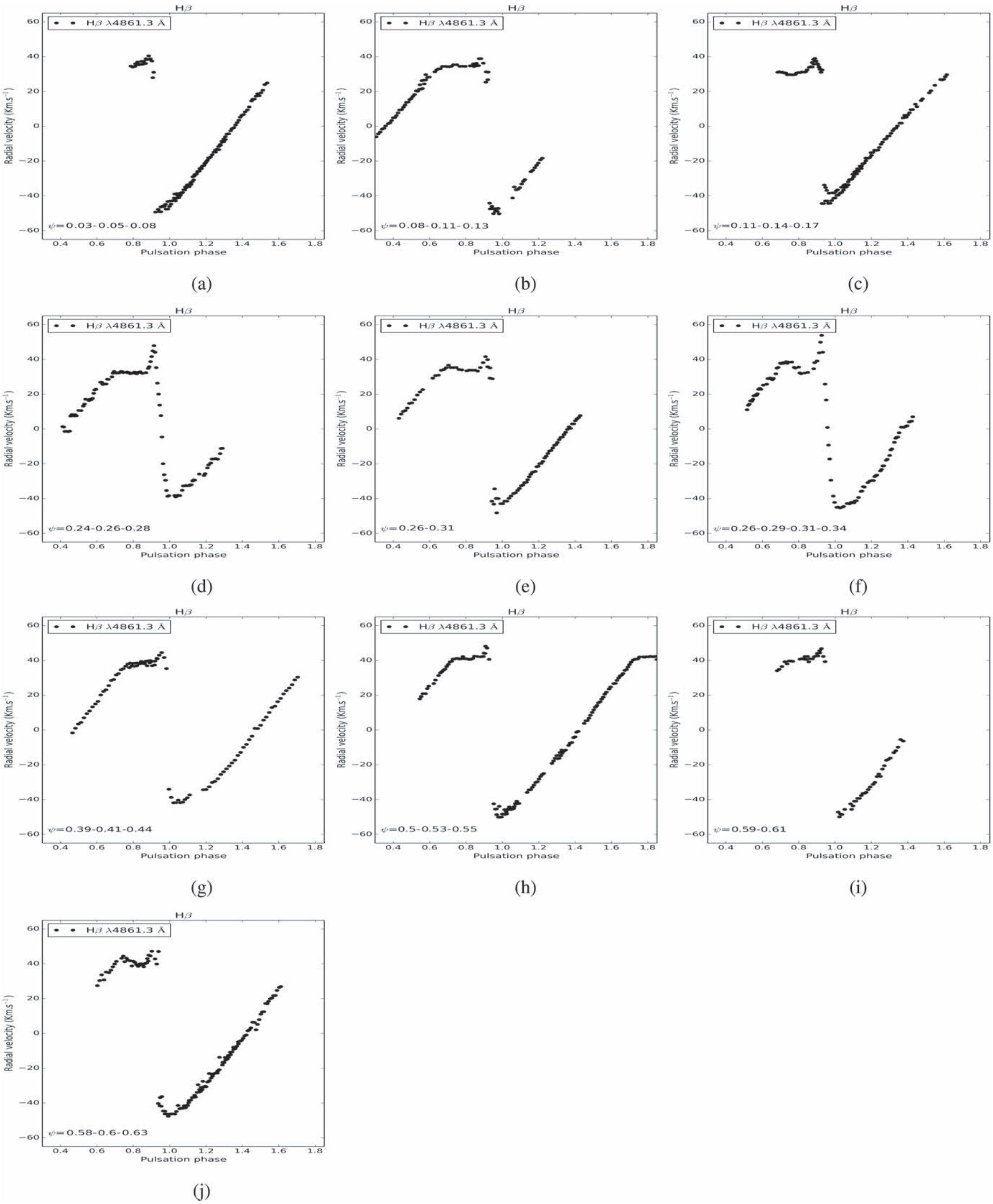

Figure 7. Same as Figure 6, but for H_β (λ4861.3 Å).

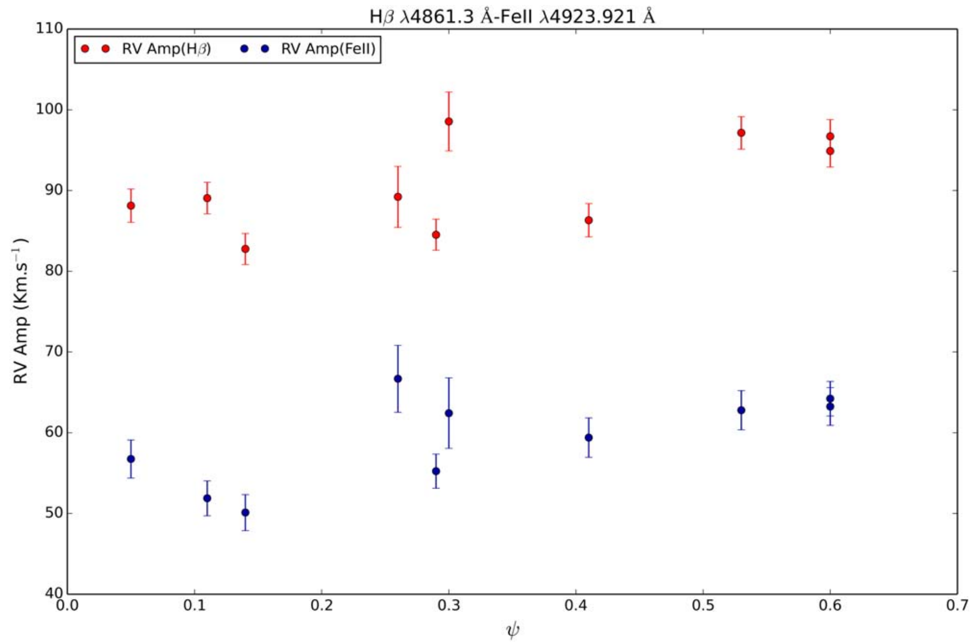

Figure 8. Amplitudes of radial velocity curves of H_β (λ4861.3 Å) and Fe II (λ4923.921 Å) lines as a function of Blazhko phases. In red are the amplitudes of the radial velocity curves of H_β and in blue those of Fe II.

Table 3
Comparison of Calculated Blazhko Phases

Date (yyyy/mm/dd)	ψ (Our calculations)	ψ (Gillet et al. 2017 and Gillet et al. 2019)	ψ (Chadid & Gillet 1997; Chadid et al. 1999, and Chadid 2000)
1994/08/03	0.39	0.39	···
1994/08/04	0.41	···	24.95
1994/08/05	0.44	···	···
1996/07/31	0.03	···	···
1996/08/01	0.05	···	16.32
1996/08/02	0.08	0.08	···
1996/08/09	0.26	···	16.55
1996/08/11	0.31	···	···
1997/06/24	0.08	···	···
1997/06/25	0.11	···	15.42
1997/06/26	0.13	···	···
1997/08/05	0.50	0.50	···
1997/08/06	0.53	···	15.42
1997/08/07	0.55	···	···
1997/08/08	0.58	···	···
1997/08/09	0.60	0.61	25.47
1997/08/10	0.63	···	···
1997/08/29	0.11	···	···
1997/08/30	0.14	0.14	25.98
1997/08/31	0.17	···	···

observation is consistent with the significant remark we previously made in Section 3 above.

Previous studies have explored the relationship between pulsation velocity and visual luminosity curves in RR Lyrae stars. These studies aimed to generate synthetic radial velocity curves, refine systemic velocity estimates, and advance our comprehension of the Galactic halo. These findings hold significant implications for large-scale cosmological surveys. Liu's work in Liu (1991) and Sesar's research in Sesar (2012) represent notable contributions to this area. Nevertheless, it is worth noting that none of these studies delved into the variability of radial velocity amplitude concerning Blazhko phases.

Figure 10 highlights the evolution of the amplitudes of the radial velocity curves of the Fe II and H_β lines as a function of time. We have adjusted this evolution by linear regression and we show that they remain almost stagnant over time (1994, 1995, 1996, 1997, 2015, 2016). It seems that, despite the evanescence of the Blazhko effect observed by Le Borgne et al. (2014), the evolution of these amplitudes has not undergone this effect. Further measurements of this effect are needed to draw a convincing conclusion about it.

Figure 11 displays the evolution of the shift between the maximum of the radial velocity curves between the lines of Fe II (λ4923.921 Å) and those of H_β (λ4861.3 Å) around the pulsation phases $\phi \approx 0.9$. We find that this offset is about 17.16 ± 2.16 km s^{-1} for the Blazhko cycle minima and about 14.23 ± 2.12 km s^{-1} for the Blazhko cycle maxima. It seems that this shift between the maximum of the radial velocity curves between Fe II and H_β is inversely correlated with the Blazhko phases. This result is in agreement with the evolution concerning the amplitudes of the radial velocity curves (Figures 8 and 9). Although we have the results deduced only from ten series of night of measurements, we think that to confirm the result of this inverse correlation we must carry out new high quality observational campaigns on other Blazhko cycles to enable us to provide a statistical conclusion relevant to this correlation.

6. Discussion

According to the graphs of the figures presented above, we discuss the physical interpretation of the results obtained. We notice that the Van Hoof effect takes place in the lower atmosphere in a significant way in agreement with the conclusions deduced from the measurements carried out by Chadid & Gillet (1998). This is observed on some Fe II-Fe II, Fe II-Fe I, Fe II-Ba II and Fe II-Ti II diagrams (Figures 1: (b), (e), (g), and (h), Figures 2: (a), (c), (d), (e), (f), (g), and (h), Figures 3: (d), (e), (f), and (g), and Figures 4: (c), (d), (f), and (g)). In the lower atmosphere, we notice that the Van Hoof effect between the metallic lines is clearer during the minimum Blazhko phases for all the RV–RV diagrams except the Fe II (λ4923.921 Å)–Fe II (λ4549.214 Å) diagram which shows a slight effect. On one hand, at the maximum of the Blazhko cycle, we find that the Van Hoof effect is generally slight or even absent between the radial velocity curves of Fe II (λ4923.921 Å)–Fe I (λ4920.509 Å), Fe II (λ4923.921 Å)-Ba II (λ4934.076 Å), and the Fe II(λ4923.921 Å)-Ti II (λ5188.7 Å). On the other hand, the shift between the radial velocity curves is absent in the Fe II(λ4923.921 Å)–Fe II (λ4549.214 Å) diagram (Figures 1: (a), (b), (d), and (f)). The conclusion that can be drawn from these observations is that the shock wave, at the minimum of the Blazhko cycle, is weaker and therefore takes much longer to traverse the lower atmospheric layers. Thus, the observed shift between the radial velocity curves is greater. On the other hand, the Van Hoof effect is weak, or even absent for the maximum Blazhko phases, where the shock waves are strong and therefore traverse the lower atmospheric layer more quickly. Consequently, they have less time to carry in their wake the different atmospheric layers. This proposition of a simplistic interpretation of this too complex and nonlinear phenomenon of the shock wave propagation in the atmosphere of pulsating stars helps us better understand the correlation that we have just discovered. For the case of Fe II (λ4923.921 Å)–Fe II(λ4549.214 Å) one could explain the absence of the Van Hoof effect between these layers for the maximum Blazhko and its weak appearance for the minimum Blazhko by the fact that the two layers containing these elements are at altitudes sufficiently close to each other to generate such an effect. From all the above, we deduce that the atmospheric layers, where the different metallic lines are formed, are not at the same altitude. Regarding the Fe II (λ4923.921 Å)-H_β (λ4861.3 Å) diagrams (Figures 5: (a), (b), (c), (d), (e), (f), (g), (h), and (i)), the Van Hoof effect is clearly evident around the pulsation phase $\phi \approx 0.9$, because the hydrogen nucleus formation layer is found in the upper atmosphere while Fe II lines are formed in the lower atmosphere. This result is consistent with those obtained by Mathias et al. (1995).

We also found a clear correlation of the Van Hoof effect with the Blazhko phase between the different metallic lines on the one hand and on the other hand between these metallic lines and H_β. This correlation is highlighted by bringing into play the amplitudes and shifts of the radial velocity curves of the different chemical elements constituting the different atmospheric layers.

The lower and upper atmospheric layers of the star RR Lyr are characterized by the presence of the chemical elements Fe II (λ4923.921 Å) and hydrogen H_β (λ4861.3 Å) respectively. The radial velocity curves deduced from the Fe II and H_β metallic lines as a function of the Blazhko phases show an inverse correlation (Figures 6 and 7). Indeed, for the maximum phases of the Blazhko cycle the radial velocity is minimum and vice versa. This finding is the same for the amplitudes of these radial velocity curves (Figures 8 and 9). These results are in

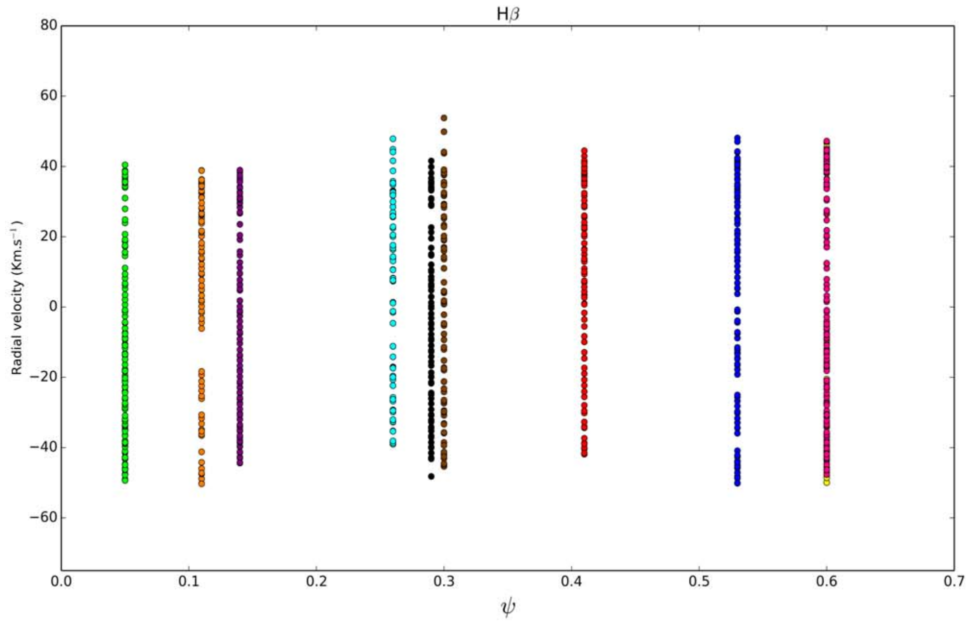

(a)

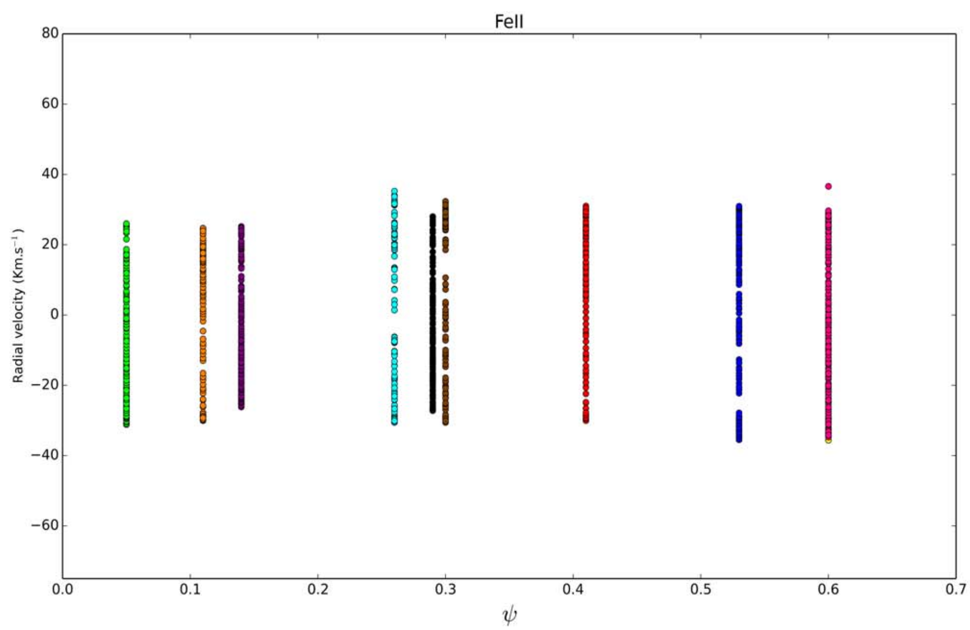

(b)

Figure 9. Evolution of radial velocity amplitudes: (a) derived from H_β lines and (b) derived from Fe II (λ4923.921 Å) lines. The *y*-axis represents the radial velocity, while the *x*-axis represents the Blazhko phases.

harmony with what has been observed on the behavior of the emission intensity of the helium D3 line as a function of the Blazhko phase ((Sefyani et al. 2020), (Benhida et al. 2020)). In their work we found that the emission intensities of the D3 line (Figure 1) are weak for the maximum of the Blazhko cycle and strong for the minima. However, a maximum Blazhko cycle implies the presence of a strong shock wave which crosses the atmosphere of the star and vice versa. We believe that this phenomenon can also be observed for the emission of the hydrogen H_β line during the $\phi \approx 0.9$ phase of the pulsation

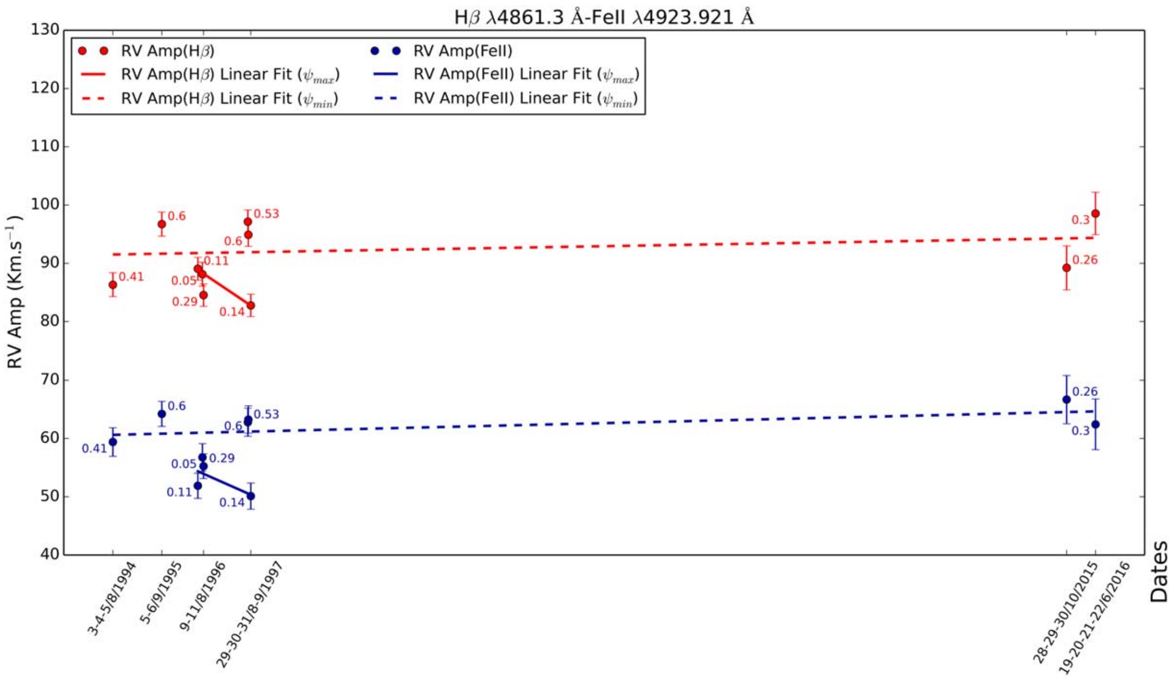

Figure 10. Amplitudes of the radial velocity curves deduced from the H_β (λ4861.3 Å) lines and those of Fe II (λ4923.921 Å) as a function of time. In red are the amplitudes of the radial velocity curves of H_β and in blue those of Fe II. The dates (dd/mm/yyyy) of the series of nights are indicated in labels on the abscissa axis. Some dates are hidden because of overlapping labels. The dashed lines are the linear fit of the amplitudes of the radial velocity curves associated with the Blazhko minima, while the continuous lines are the linear fit of the amplitudes corresponding to the Blazhko cycle maxima. Blazhko phases are indicated on the graph.

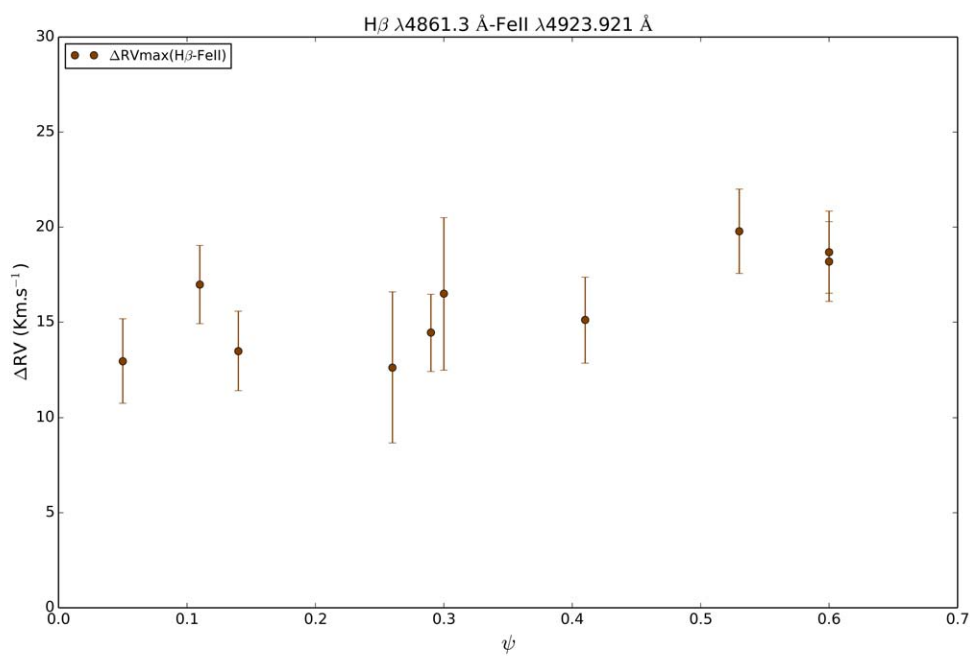

Figure 11. Shift between the maximum of the radial velocity curves (around the pulsation phase $\phi \approx 0.9$) of the H_β (λ4861.3 Å) lines and those of Fe II (λ4923.921 Å) as a function of the Blazhko phases.

cycle. We mention that this phenomenon was observed in the RV Tauri star R Scuti (R Sct) in which the emission intensity of the H_α line is decreasing for strong shock waves and vice versa (Chafouai et al. 2022). The phenomenon of ionization is probably responsible for this mechanism. In fact the stronger the shock wave is, the more hydrogen that is ionized which can therefore no longer participate in the emission of Balmer lines with low emission intensity. According to this hypothesis, a strong shock wave is generated in its wake (Gillet & Lafon 1983) accompanied by a strong ionization and, after recombination, a stronger photometric emission is observed at the pulsation phase 0.9. However, a strong photometric emission generates a compression on the atmospheric gas.

Fadeyev & Gillet (2004) theoretically studied the structure of equilibrium radiative shock waves propagating through ionized hydrogen gas at the temperature of 3000 K in stars of density 10^{-12} g cm$^{-3} \leqslant \rho_1 \leqslant 10^{-9}$ g cm^{-3}. The most remarkable result of this study is that the shock wave patterns show the dual emission structure in the H_α and H_β profiles of the emergent radiation flux that is well known from high resolution, high SNR spectroscopy. Another important conclusion is that the velocity deduced from the Doppler shifts of the Balmer lines is about one third of the velocity of the shock wave. This is because the layers of gas emitting the Balmer line radiation are located behind the shock wave in the hydrogen recombination region where the velocity in the observer's Stellar Rest Frame is about half the velocity of the shock wave. In this work Fadeyev & Gillet (2004) showed that a strong Balmer radiative pressure generated during the photometric maximum ($\phi \approx 0.9$) generates a strong compression on the atmospheric gas. Consequently, we believe that this radiative compression causes a slowing down of the movement speeds of the different atmospheric layers during each pulsation cycle. This slowing of the displacement of these layers induces a lower radial velocity amplitude during the maximum of the Blazhko cycle where the shock waves are strong (Figures 6, 7, 8, and 9).

The same physical phenomenon which interprets the evolution of the amplitudes of the radial velocities of Fe II and H_β with respect to the Blazhko cycles also makes it possible to explain the evolution of the shift between the maximum radial velocities of these two elements (Figure 11). A maximum phase of the Blazhko cycle generates a small shift between the maximum radial velocities of Fe II and H_β which are at the extremities of the atmosphere of the star.

7. Conclusion

Our observations on the recorded spectra of the star RR Lyr highlight the existence of a correlation between the Blazhko effect and the Van Hoof effect. We observed the Van Hoof effect between Fe II (λ4923.921 Å)–Fe II (λ4549.214 Å), Fe II (λ4923.921 Å)–Fe I (λ4920,509 Å), Fe II (λ4923.921 Å)–Ba II (λ4934,076 Å), Fe II (λ4923.921 Å)–Ti II (λ5188.7 Å) and Fe II (λ4923.921 Å)-H_β (λ4861.3 Å) during different Blazhko cycles. An inverse correlation between the Van Hoof effect and the Blazhko effect has been observed, which stipulates that during the maximum of the Blazhko cycle, a propagation of shock waves leads to a strong radiative pressure which in turn causes a strong slowing down of the movement of the different atmospheric layers and consequently a decrease in the amplitudes of the radial velocities. This decrease in radial velocities is responsible for this inverse correlation effect between the Blazhko effect and the Van Hoof effect observed at different phases of the Blazhko cycle. It can be concluded that shock waves play a key role in understanding the atmospheric dynamics of the star RR Lyr. Additionally, we assume that radiative pressure is significant in this star compared to other stars of the same type, although confirming this hypothesis requires more observations of RR Lyr and other stars in the same class. All of these results contribute quantitatively to validating the implications of the theoretical results of the nonlinear models that govern the atmospheric dynamics of pulsating stars.

Acknowledgments

We thank Gillet Denis very much for allowing us to download and use the OHP spectroscopic data, observed by him and Meriem Chadid. We also thank Storm Brabants for proofreading the article.

Appendix

Table A1
Summary Table of Blazhko Phases Calculated Using the Ephemerides HJD Max Light Below (Chadid & Gillet 1996 and Gillet et al. 2017)

Date (yyyy mm dd)	Nbr of spectra	Nbr Blazhko Cycle	Period (days)	HJD max light	Phase ψ
1994 Aug 3	26	0	39.03	2449631.312	0.39
1994 Aug 4	35	0	39.03	2449631.312	0.41
1994 Aug 5	34	0	39.03	2449631.312	0.44
1995 Sep 5	48	8	39.03	2449943.552	8.59
1995 Sep 6	12	8	39.03	2449943.552	8.62
1996 Jun 24	30	16	39.06	2450256.272	16.08
1996 Jun 25	34	16	39.06	2450256.272	16.11
1996 Jun 26	30	16	39.06	2450256.272	16.13
1996 Jul 31	52	17	39.06	2450295.332	17.03
1996 Aug 1	56	17	39.06	2450295.332	17.05
1996 Aug 2	20	17	39.06	2450295.332	17.08
1997 Aug 5	37	26	39.06	2450646.872	26.5
1997 Aug 6	58	26	39.06	2450646.872	26.53
1997 Aug 7	56	26	39.06	2450646.872	26.54
1997 Aug 8	60	26	39.06	2450646.872	26.57
1997 Aug 9	48	26	39.06	2450646.872	26.6
1997 Aug 10	38	26	39.06	2450646.872	26.63
1997 Aug 29	51	27	39.06	2450685.932	27.11
1997 Aug 30	65	27	39.06	2450685.932	27.14
1997 Aug 31	60	27	39.06	2450685.932	27.17
2015 Oct 28	42	0	39.00	2457354.322	0.24
2015 Oct 29	57	0	39.00	2457354.322	0.26
2015 Oct 30	60	0	39.00	2457354.322	0.28
2016 Jun 19	66	5	39.00	2457354.322	5.26
2016 Jun 20	75	5	39.00	2457354.322	5.29
2016 Jun 21	23	5	39.00	2457354.322	5.31
2016 Jun 22	35	5	39.00	2457354.322	5.34

ORCID iDs

Y. El jariri https://orcid.org/0000-0003-1744-4743

References

Baranne, A., Queloz, D., Mayor, M., et al. 1996, A&AS, 119, 373
Benhida, A., Sefyani, F. L., Benkhaldoun, Z., et al. 2021, in ASP Conf. 529, RR Lyrae/Cepheid 2019: Frontiers of Classical Pulsators, ed. K. Kinemuchi et al. (San Francisco, CA: Astronomical Society of the Pacific), 11
Blažko, S. 1907, AN, 175, 325
Burki, G., Mayor, M., & Benz, W. 1982, A&A, 109, 258
Chadid, M., & Gillet, D. 1996, A&A, 308, 481
Chadid, M., & Gillet, D. 1997, A&A, 319, 154
Chadid, M., & Gillet, D. 1998, A&A, 335, 255
Chadid, M., Kolenberg, K., Aerts, C., & Gillet, D. 1999, A&A, 352, 201
Chadid, M. 2000, A&A, 359, 991
Chadid, M., & Preston, G. W. 2013, MNRAS, 434, 552
Chadid, M. 2023, ApJ, 951, 127
Chafouai, K., Benhida, A., Sefyani, F. L., et al. 2022, ARep, 66, 1276
Dalmazio, D. 1992, GEOS Circ. 678, 1
Dalmazio, D. 1995, GEOS Circ. 773, 1
El Jariri, Y., Sefyani, F. L., Benhida, A., et al. 2023, A&C, 43, 100708
Fadeyev, Y. A., & Gillet, D. 2004, A&A, 420, 423
Fleming, W. P. 1899, Project PHAEDRA: Preserving Harvard's Early Data and Research in Astronomy, 14, 815
Fokin, A. B. 1992, MNRAS, 256, 26
Fokin, A. B., & Gillet, D. 1997, A&A, 325, 1013
Gillet, D., & Lafon, J.-P. J. 1983, A&A, 128, 53
Gillet, D., Sefyani, F. L., Benhida, A., et al. 2016, A&A, 587, A134
Gillet, D., Mauclaire, B., Garrel, T., et al. 2017, A&A, 607, A51
Gillet, D., Mauclaire, B., Lemoult, T., et al. 2019, A&A, 623, A109
Le Borgne, J.-F., Poretti, E., Klotz, A., et al. 2014, MNRAS, 441, 1435
Liu, T. 1991, PASP, 103, 205
Mathias, Ph., & Gillet, D. 1993, A&A, 278, 511
Mathias, P., Gillet, D., Fokin, A. B., & Chadid, M. 1995, A&A, 298, 843
Preston, G. W. 2011, AJ, 141, 6
Sefyani, F. L., Benhida, A., Benkhaldoun, Z., et al. 2017, JPhCS, 869, 012088
Sefyani, F. L., Benhida, A., Benkhaldoun, Z., et al. 2018, in Proc. Polish Astronomical Soc. 6, The RR Lyrae 2017 Conference. Revival of the Classical Pulsators: from Galactic Structure to Stellar Interior Diagnostics, ed. R. Smolec, K. Kinemuchi, & R. I. Anderson (Warsaw: Polish Astronomical Society), 316
Sefyani, F. L., Benhida, A., Benkhaldoun, Z., et al. 2021, in ASP Conf. 529, RR Lyrae/Cepheid 2019: Frontiers of Classical Pulsators., ed. K. Kinemuchi et al. (San Francisco, CA: Astronomical Society of the Pacific), 343
Sesar, B. 2012, AJ, 144, 114
Shapley, H. 1916, ApJ, 43, 217
Thizy, O., & Cochard, F. 2011, in IAU Symp. 272, Active OB Stars: Structure, Evolution, Mass Loss, and Critical Limits (Cambridge: Cambridge Univ. Press), 282
Van Hoof, A., & Struve, O. 1953, PASP, 65, 158